

LETTER TO THE EDITOR

# Radiation-pressure instability is an artifact of constant- $\alpha$ closure

## Implications for AGN disk tensions

M. H. Naddaf<sup>1</sup>, M. Ghasemnezhad<sup>2</sup>, H. Ghanbarnejad<sup>2</sup>, D. Hutsemékers<sup>1</sup>, and B. Czerny<sup>3</sup>

<sup>1</sup> Institut d'Astrophysique et de Géophysique, Université de Liège, Allée du six août 19c, B-4000 Liège (Sart-Tilman), Belgium

<sup>2</sup> Department of Interdisciplinary Physics and Technology, Faculty of Science, Shahid Bahonar University of Kerman, Kerman, Iran

<sup>3</sup> Center for Theoretical Physics, Polish Academy of Sciences, Al. Lotników 32/46, 02-668 Warsaw, Poland

July 1, 2026

### ABSTRACT

**Aims.** The standard  $\alpha$ -disk formalism parametrizes turbulent angular momentum transport through a dimensionless coefficient  $\alpha$ , assumed to be spatially and thermodynamically invariant. While analytically convenient, this assumption leads to the well-known thermal and viscous instabilities in radiation-pressure dominated (RPD) regions. We show that this instability is not the consequence of radiation pressure, but is due to enforcing a constant  $\alpha$  across distinct thermodynamic regimes.

**Methods.** Requiring the steady thin-disk (TD) to remain thermally stable and single-valued in the  $\dot{M}$ - $\Sigma$  plane yields a necessary condition on the stress response, expressed as  $\eta_x \equiv d \ln \alpha_x / d \ln X > 4/7$ , where  $X \equiv P_{\text{gas}}/P_{\text{rad}}$ . The resulting viscosity law  $\alpha_x \equiv \alpha(X)$  emerges directly from the internal consistency of TD equations, without modifying the stress law or invoking any additional physics.

**Results.**  $\alpha_x$  removes the RPD unstable branch. The disk structure becomes smooth and globally single-valued, with higher  $\Sigma$  and  $\tau$  in the inner RPD disk, while preserving the standard effective-temperature profile. This increases thermal and inflow timescales, offering a natural route to accretion-state dependent variability without large-amplitude radiation-pressure limit cycles. It also motivates revisiting AGN disk tensions, including microlensing sizes and continuum reverberation lags with improved radiative-transfer modeling. The results show that the RPD instability, and possibly some associated AGN disk tensions, reflect an inconsistent viscosity closure.

**Key words.** accretion, accretion disks – instabilities – black hole physics – radiation mechanisms: general – methods: analytical

## 1. Introduction

The standard TD model of Shakura & Sunyaev (1973) remains the canonical framework for describing radiatively efficient accretion onto compact objects and underlies much of the standard interpretation of active galactic nuclei and black hole growth (Netzer 2013). Its central simplification is the replacement of the unknown transport physics by a local closure, in which the turbulent stress is set as a fraction of the local pressure via the dimensionless parameter  $\alpha$ . This prescription yields the familiar analytic structure equations and has underpinned much of modern accretion theory. Yet, it leaves unresolved the basic physical question of why the effective stress should remain independent of the local thermodynamic regime (Pringle 1981). The RPD regions being thermally and viscously unstable when the stress scales with total pressure, is the classical Lightman & Eardley (1974) instability, later developed by Shakura & Sunyaev (1976) and generalized by Piran (1978); The  $\dot{M}$ - $\Sigma$  equilibrium curve then develops a negative-slope segment, producing the familiar unstable branch and motivating long-standing discussions of large-amplitude disk variability and limit-cycle behavior. The physical origin of this instability however remained uncertain, as constant  $\alpha$  is not a prediction of disk microphysics.

In sufficiently ionized disks, angular momentum transport is expected to arise from MHD turbulence driven by magnetorotational instability (MRI), rather than from a universal hydrodynamic viscosity (Balbus & Hawley 1991; Hawley et al. 1995). Thus,  $\alpha$  should be regarded as an effective closure parameter describing the nonlinear saturation of MRI, which may depend on

the disk thermodynamic state. There is thus no *a priori* reason for  $\alpha$  to remain invariant across the transition from gas-pressure dominated (GPD) to RPD regimes. Early magnetic-viscosity arguments already suggested that the inner RPD disk need not follow the naive total-pressure stress law (Sakimoto & Coroniti 1981). GRMHD simulations likewise indicate that  $\alpha$  need not be spatially constant Penna et al. (2013); Abramowicz et al. (2026).

This is reinforced by empirical, observational, and theoretical studies of thin, fully ionized disks showing that  $\alpha$  is not universal. Typical values are of order  $\alpha \sim 0.1$ , while viable observational and numerical ones span  $10^{-4} \lesssim \alpha \lesssim 0.3$  (King et al. 2007; Hirose et al. 2009). More importantly, radiation-MHD simulations show that the RPD regime can deviate from constant- $\alpha$  models (hereafter SS models). Stratified shearing-box calculations by Hirose et al. (2009) found no catastrophic thermal runaway showing that stress fluctuations can precede pressure fluctuations, challenging the interpretation of stress as a local function of total pressure. Larger-box simulations recover runaway behavior, but with heating, cooling, and vertical energy transport largely different from the SS expectations (see e.g., Jiang et al. 2013a, 2019). The central issue is thus whether a rigid SS closure is internally consistent for RPD MRI (Blaes et al. 2025).

Proposed remedies include gas- or mixed-pressure scaling in the stress law (Sakimoto & Coroniti 1981; Stella & Rosner 1984; Merloni & Nayakshin 2006); introducing magnetically elevated or supported disks that alter the vertical structure and pressure balance (Begelman & Pringle 2007; Sadowski 2016b); incorporating wind-driven mass-loss that changes the local  $\dot{M}$  and  $\Sigma$  structure (Poutanen et al. 2007; Laor & Davis 2014;

arXiv:2606.31998v1 [astro-ph.HE] 30 Jun 2026

Habibi & Abbassi 2019); or adopting slim-disk solutions in which advective cooling becomes important (Abramowicz et al. 1988; Chen et al. 1995). These approaches, although valuable (e.g., Lightman & Eardley 1974; Zheng et al. 2011), weaken the heating response in RPD regions by construction. In practice, they modify the stress law phenomenologically, invoke additional physics, or leave the standard TD branch.

Our approach here is minimal. We retain the standard TD equations and ask what dependence of  $\alpha$  on the local thermodynamic state is required for a steady, self-consistent, and globally stable solution, without introducing additional physics. Unlike other prescriptions, the present form is not guessed, assumed, or imposed independently, but derived as a necessary condition required by TD equations. Defining  $X \equiv P_{\text{gas}}/P_{\text{rad}}$ , we derive  $\alpha_x$  by requiring both thermal stability of the local equilibrium solution and a single-valued  $\dot{M}$ - $\Sigma$  relation. The viscosity law thus emerges from the internal structure of standard TD framework.

This Letter shows that the SS closure is internally inconsistent in the RPD TD. Consistency imposes a lower bound on the logarithmic response of  $\alpha$  to the  $X$ . Once this bound is satisfied, the classical unstable branch disappears while the analytic TD structure is preserved. Thus, the RPD instability is not the consequence of radiation support, but is an artifact of enforcing an inconsistent closure across distinct thermodynamic regimes.

The paper is organized as follows. In Section 2 we introduce the consistent  $\alpha_x$  closure derived from both the local thermal stability criterion and the structure of the  $\dot{M}$ - $\Sigma$  equilibrium curve. In Section 3 we show how it removes the classical unstable branch and modifies the disk structure. It is followed by discussion in Section 4. We summarize the implications in Section 5.

## 2. Self-consistent $\alpha_x$ prescription

We next examine how  $\alpha_x$  affects the TD structure. We use the classical height-integrated, steady-state Shakura & Sunyaev (1973) framework, adopting Newtonian gravity for simplicity. The only new element is that  $\alpha$  is no longer constant, but depends on the local pressure partition  $X$ , as

$$\alpha_x \equiv \alpha(X), \quad \text{where} \quad X \equiv P_{\text{gas}}/P_{\text{rad}}. \quad (1)$$

A regime-dependent  $\alpha$  is a physically natural expectation rather than a new hypothesis. The novelty here is to examine this previously unexplored dependence explicitly and determine the behavior required for a globally thermally stable TD solution.

A simple sufficient form that satisfies the stability condition (see the Appendix A for derivations) is a power-law

$$\alpha_x = \alpha_0 X_x^p, \quad \text{with} \quad p > 4/7 \quad (2)$$

where  $\alpha_0$  is a normalization factor.

The required response is derived from the condition that the equilibrium branch remain stable and single-valued. The result is not an ad hoc modification, but a constraint on the effective closure itself: any proposed stress prescription must have an effective  $\eta_x > 4/7$  to avoid the classical RPD unstable branch.

## 3. Results

Figure 1 shows how  $\alpha_x$  determines whether the classical unstable branch exists. It summarizes the behavior of disk solutions as a function of the slope  $p$  in the emergent viscosity law  $\alpha_x \propto X^p$ , for  $M_\bullet = 10^8$  at  $r = 20$ , where  $M_\bullet = M_{\text{bh}}/M_\odot$  is the black hole mass in solar unit, and  $r = R/R_g$  is the dimensionless radius with  $R_g = GM_{\text{bh}}/c^2$  the gravitational radius.

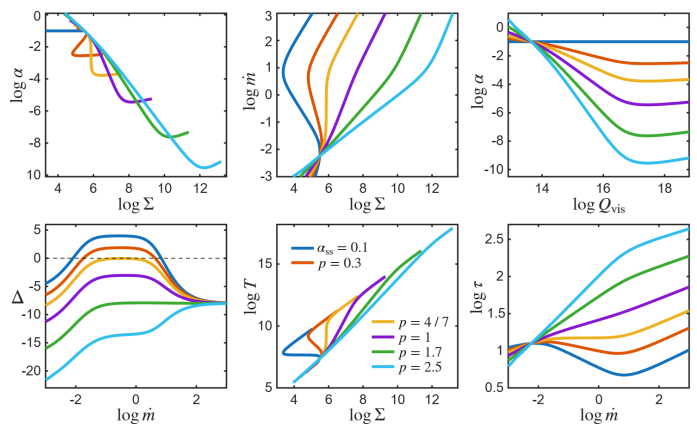


**Fig. 1.** The disk thermal–viscous stability with regime-dependent  $\alpha$ , for  $M_\bullet = 10^8$  at  $r = 20$ . Multi-panel view of steady-state TD solutions (in cgs units) computed with  $\alpha_x = \alpha_0 X^p$  (with arbitrarily  $\alpha_0 = 0.1$ ). Colors denote different indices  $p$  as labeled; SS model ( $p = 0$ ) is labeled as  $\alpha_{\text{ss}} = 0.1$ . The equilibrium S-curves in the  $\Sigma$ - $\dot{M}$  plane (expressed in Eddington unit as  $\dot{m} = \dot{M}/\dot{M}_{\text{Edd}}$ ) is shown in *top middle* panel; the characteristic middle (unstable) branch present for  $\alpha_{\text{ss}}$  flattens with increasing  $p$  and disappears for  $p \gtrsim 4/7$ .  $\Delta$  is the thermal stability diagnostic shown in *bottom left* panel; the unstable regime ( $\Delta > 0$ ) progressively shrinks as  $p$  increases and vanishes for  $p \gtrsim 4/7$ . *Bottom middle* panel shows that the multi-valued structure of temperature solutions collapses to a single monotonic branch as the disk becomes globally stable. *Bottom right* panel shows a monotonically increasing trend with  $\dot{m}$  for stabilized disk, with significant enhancement of optical thickness (and thus  $\Sigma$ ) in the inner disk, compared to standard SS model.

The top-left panel shows the effective  $\alpha$  versus  $\Sigma$ . The larger the  $p$  is, the more rapidly  $\alpha$  declines, suppressing viscosity in RPD regimes. The global effect is shown in the top-middle panel. For small  $p$ , the classical S-shaped  $\dot{M}$ - $\Sigma$  relation of RPD TD is recovered (Shakura & Sunyaev 1973; Lightman & Eardley 1974). As  $p$  increases, the unstable middle branch shrinks, disappears for  $p > 4/7$ , the sequence becomes monotonic, removing the thermal-viscous instability. This agrees with earlier expectations that a strong decline in  $\alpha$  in RPD regime suppresses the heating-cooling runaway (e.g., Stella & Rosner 1984), but here follows directly from TD equations. The top-right panel shows  $\alpha$  versus viscous heating, revealing the weakened heating response that stabilizes the RPD branch.  $\alpha$  falls steeply at low  $Q_{\text{vis}}$ , then shows an inflection and flattens at high  $Q_{\text{vis}}$ , reflecting changes in the dominant opacity and cooling mechanisms. The bottom-middle panel shows the corresponding temperature profiles. For low  $p$ , the turning point of the unstable branch remains visible, whereas for larger  $p$  the profiles become smooth and single-valued. Thus, the disappearance of the S-curve reflects a continuous thermodynamic structure rather than a jump between branches. The bottom-left panel shows the thermal stability parameter  $\Delta$ . For small  $p$ ,  $\Delta$  becomes positive over a finite range of  $\dot{M}$ , recovering the classical instability criterion. As  $p$  increases, the peak of  $\Delta$  drops and eventually remains negative for all  $\dot{M}$ , demonstrating global thermal stability. The critical value  $p = 4/7$  thus emerges as the lower bound for marginal stability. The bottom-right panel shows  $\tau$  versus  $\dot{m}$ . For stabilized disks,  $p > 4/7$ , the optical depth increases monotonically with  $\dot{m}$ . At fixed  $\dot{m}$  above  $\sim -2$  dex, larger  $p$  gives systematically higher  $\tau$ , reflecting the stronger temperature and density dependence of the opacity. The curves also steepen at high  $\dot{m}$  as the disk enters the RPD regime and the opacity approaches electron scattering.

Taken together, the figure shows that  $\alpha_x$  is not arbitrary: thermal equilibrium and stability require a regime-dependent stress response that recovers the classical unstable behavior for shallow slopes, but removes it above the critical slope. This provides a physically motivated route to stabilizing RPD disks without strong magnetic support or ad hoc stress prescriptions (e.g., Jiang et al. 2013b,a; Sadowski 2016b,a), emphasizing the role of pressure partition,  $X$ , in regulating angular momentum transport.

## 4. Discussion

### 4.1. Implications for accretion studies

The main result is that the classical radiation-pressure instability need not be intrinsic to radiation-supported accretion flows. Requiring the TD equations to remain thermally stable and single-valued in  $\dot{M}$ – $\Sigma$  plane forces the viscosity to respond to the local  $X$ . The instability is thus removed not by adding new physics, but by enforcing internal consistency in the standard TD framework.

This places our result within the classical stability problem. The original instability was derived within the SS framework (Lightman & Eardley 1974; Shakura & Sunyaev 1976), while Piran (1978) emphasized that stability depends on the adopted heating and cooling closure. Our derivation sharpens this point by showing that the closure itself is constrained by the requirement that the equilibrium branch remain physically admissible.

This differs from earlier stabilization strategies. Gas-pressure or mixed-pressure prescriptions, including magnetically motivated variants, soften the stress response through assumed stress laws (Sakimoto & Coroniti 1981; Merloni & Nayakshin 2006; Grzedzielski et al. 2017); slim disks move to an advective branch (Abramowicz et al. 1988); and magnetically supported disks alter vertical support and stress balance (Begelman & Pringle 2007; Sadowski 2016b). By contrast, we show that even within the standard SS equations, the  $\alpha_{ss}$  closure is not self-consistent once radiation pressure becomes dynamically important.

The MRI context makes such a conclusion natural. Since angular momentum transport is MRI-driven (Balbus & Hawley 1991; Hawley et al. 1995),  $\alpha$  should describe the saturated turbulence rather than act as a fundamental constant. It may thus depend on whether the disk is GPD or RPD, and on radiative diffusion, buoyancy, and vertical energy transport (Blaes & Socrates 2001). Without MRI saturation modeling, we identified the effective closure required for TD consistency.

This interpretation is broadly consistent with radiation-MHD simulations (Hirose et al. 2009; Jiang et al. 2013b, 2019), showing that a total-pressure closure is incomplete. More generally, radiation-MHD stresses are time-dependent, spatially variable, and not instantaneous functions of local pressure. Our result suggests that instability persists only when the effective stress responds too weakly to changes in the local pressure partition.

Future work should connect this framework to advective, quasi-spherical, outflowing, and magnetically influenced accretion regimes (Narayan & Yi 1994; Abramowicz et al. 1995; King et al. 2007; Mosallanezhad et al. 2014). AGN extensions should include opacity effects, especially the iron-opacity bump, time-dependent evolution with  $\alpha_x$  across RPD and unstable zones, and direct comparisons with 3D radiation-MHD simulations (e.g., Jiang et al. 2016; Jiang et al. 2019).

### 4.2. Implications for AGNs

Observed AGN disks already show tensions with the simplest TD predictions, but the main implication of the present closure

is more basic: an RPD disk need not become low-column, thermally unstable, advective, or geometrically inflated. If the stress follows the local thermodynamic regime, the disk can remain RPD, optically thick, and thermally stable. The closure does not remove radiation pressure; it changes the disk response to it.

The structural reason is direct. In RPD regions, where  $X$  is small,  $\alpha_x$  is reduced. At fixed  $\dot{m}$ , it is thus compensated by raising  $\Sigma$ , rather than moving onto the low-column RPD branch. This removes the unstable low- $\Sigma$  solution and enhances the inner disk optical thickness. Analytically, the deviation is controlled by  $S \propto \dot{m}^8 M_\bullet \mathcal{J}^8(r) r^{-21/2}$ , and thus grows with both  $M_\bullet$  and, more strongly,  $\dot{m}$  (see the Appendix A.5).

Because  $\alpha_x \propto X^p$  and  $X$  varies with radius, the closure also produces a self-consistent radial viscosity profile, as an analytic analog of empirical or simulation-calibrated  $\alpha(r)$  models (see e.g., Penna et al. 2013; Abramowicz et al. 2026).

This weakens the need for an early transition to a slim-disk at moderate to high  $\dot{m}$ . Stability can be obtained while remaining close to a TD-like branch, which is relevant for quasars, NLS1s, SEAMBHs, and high-redshift luminous sources whose optical/UV continua are often interpreted with TD-like scalings even at high inferred accretion rates (Done et al. 2007; Wang et al. 2014; Du et al. 2018; Czerny 2019). A suggestive example is the variable spectrum of a  $z = 6.51$  quasar accreting at  $\lambda_{\text{Edd}} \sim 0.6$ , consistent with  $\lambda F_\lambda \propto \lambda^{-4/3}$  (Leung et al. 2026). Unlike slim disks, which stabilize high-accretion flows through advection in a geometrically thicker configuration (Abramowicz et al. 1988), the present closure stabilizes the RPD branch through the stress response while preserving a thin, smooth  $H/R$  structure.

A related implication concerns variability. The classical RPD instability predicts large-amplitude burst–quench cycles, yet such cycles are rare in luminous AGNs, although they remain relevant for some extreme Galactic accretors such as GRS 1915+105 (Belloni et al. 1997; Janiuk & Czerny 2011; Śniegowska et al. 2023). Since  $\alpha_x$  reduces the heating response to the RPD state and raises  $\Sigma$  and  $\tau$ , the expected phenomenology is thus an optically thick, slowly evolving inner disk, rather than a violently intermittent one. This is qualitatively consistent with optical quasar variability studies, where damping times, variance, and power spectra depend on  $M_\bullet$ , wavelength,  $\lambda_{\text{Edd}}$ , and the probed timescale (McHardy et al. 2006; Arévalo & Uttley 2006; Kelly et al. 2009; Stone et al. 2022). The observed suppression of optical variance with increasing  $M_\bullet$  and  $\lambda_{\text{Edd}}$  provides an empirical benchmark for the predicted increase of thermal and inflow timescales in RPD disks (Arévalo et al. 2023). If the optical damping time traces the local thermal response, then  $t_{\text{th}}/t_{\text{dyn}} \sim \alpha_x^{-1}$ . For  $M_\bullet = 10^9 M_\odot$  at  $r = 20$ ,  $t_{\text{dyn}} \sim 5$  days, so a characteristic timescale  $\sim 300$  days implies  $\alpha_x \sim 0.017$ , as shown in Fig. 2.

The geometric implications are also important. The fraction of coronal radiation intercepted by the disk, BLR illumination, self-shadowing, and wind shielding all depend on  $H/R$ . Slim-disk self-shadowing models predict strong anisotropy and multiple BLR zones with different lags and line widths (Wang et al. 2014; Du et al. 2018), while line-driven wind and obscurer models depend sensitively on geometry through X-ray shielding and UV illumination (Murray et al. 1995; Proga et al. 2000; Giustini et al. 2023). In the present model, radiation pressure does not by itself force the inner disk into a puffed-up funnel. A smoother, thinner  $H/R$  profile thus implies less extreme irradiation and shielding geometry than in strongly inflated slim disks (Wang et al. 2014; Du et al. 2018), while remaining closer to the thin branch than magnetically elevated or toroidally supported disks (Begelman & Pringle 2007; Begelman & Silk 2017).

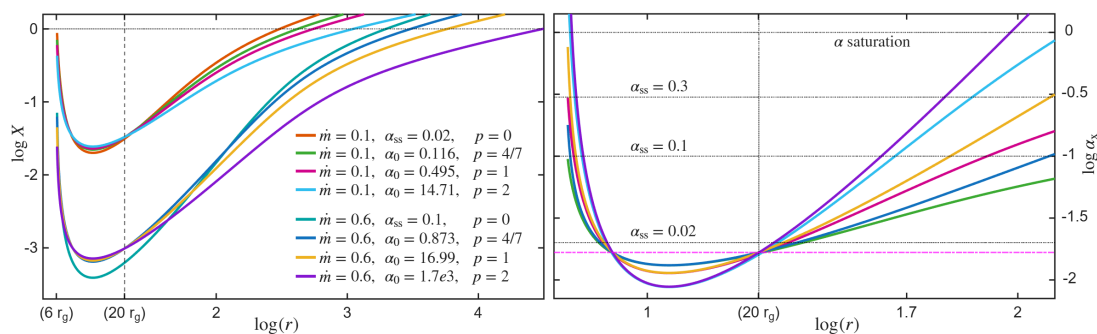


**Fig. 2.** Radial behavior of  $X$ , and  $\alpha_x^{-1}$  for  $M_* = 10^9$ . The magenta dash-dotted line mark the long-timescale variability of 300 days at  $20 r_g$ . The black horizontal dotted lines as annotated indicate different values of  $\alpha_{ss}$ , with the physical saturation threshold of viscosity parameter at the bottom. Also, the opacity is treated as  $\kappa = \kappa_{es} + \kappa_{ff}$ , where  $\kappa_{ff} = \kappa_0 \rho T^{-7/2}$ , with  $\kappa_0 = 5 \times 10^{24} \text{ cm}^5 \text{ g}^{-2} \text{ K}^{7/2}$  adopted here.

The same structural changes may affect continuum-emitting regions. Microlensing and continuum-lag studies often infer optical sizes larger than predicted by the simplest TD model, while retaining wavelength dependences broadly consistent with disk-like reprocessing (Morgan et al. 2010; Jha et al. 2022; Hutsemékers & Sluse 2025). Since the present height-integrated model essentially preserves the effective-temperature profile, it does not by itself solve the blackbody size discrepancy. Its robust implication is instead structural: larger  $\Sigma$  and  $\tau$  modify the vertical column in which the continuum is thermalized, potentially affecting color corrections, surface-brightness weighting, atmospheric thermalization depths, and lag normalization. Quantifying these effects requires disk-atmosphere and radiative-transfer calculations beyond the present treatment.

Overall, the AGN implication of the  $\alpha_x$  closure is that RPD disks can remain optically thick, stable, and TD-like while developing larger surface densities, longer response times, smoother thickness profiles, and modified illumination conditions. These changes affect precisely the inner-disk regime where variability, irradiation, winds, and continuum-size measurements are most sensitive to disk structure.

## 5. Conclusions

We have shown that internal consistency of the TD equations requires a pressure-dependent viscosity law. This preserves the analytic simplicity of the SS framework while removing the RPD instability: the unstable branch is not intrinsic to RPD disks, but due to imposing a thermodynamically invariant closure across distinct regimes. No new transport physics is introduced; the effective viscosity is simply allowed to respond to the local pressure partition, softening the heating response and restoring a single-valued TD solution.

Moreover, the  $\alpha_x$  closure smooths the scale-height response of the inner disk while raising its surface density, suggesting that moderate-to-high  $\dot{m}$  AGN disks can remain geometrically thin, optically even thicker without immediately turning slim. By lengthening both thermal and inflow timescales, it provides a natural route to accretion-state dependent variability without invoking large-amplitude radiation-pressure instability cycles. These structural changes may further affect irradiation geometry, BLR illumination, and wind launching, offering a coherent framework for luminous AGNs that remain stable despite classical SS expectations.

*Acknowledgements.* This work was supported by the F.R.S. FNRS under the research grant IISN 4.4503.19. DH is F.R.S.-FNRS Research Director.

## References

- Abramowicz, M. A., Brandenburg, A., Horák, J., et al. 2026, arXiv e-prints, arXiv:2603.10997
- Abramowicz, M. A., Chen, X., Kato, S., Lasota, J.-P., & Regev, O. 1995, The Astrophysical Journal, 438, L37
- Abramowicz, M. A., Czerny, B., Lasota, J. P., & Szuszkiewicz, E. 1988, ApJ, 332, 646
- Arévalo, P., Lira, P., Sánchez-Sáez, P., et al. 2023, MNRAS, 526, 6078
- Arévalo, P. & Uttley, P. 2006, MNRAS, 367, 801
- Balbus, S. A. & Hawley, J. F. 1991, ApJ, 376, 214
- Begelman, M. C. & Pringle, J. E. 2007, MNRAS, 375, 1070
- Begelman, M. C. & Silk, J. 2017, MNRAS, 464, 2311
- Belloni, T., Méndez, M., King, A. R., van der Klis, M., & van Paradijs, J. 1997, ApJ, 479, L145
- Blaes, O., Jiang, Y.-F., Lasota, J.-P., & Lipunova, G. 2025, Space Science Reviews, 221
- Blaes, O. & Socrates, A. 2001, ApJ, 553, 987
- Chen, X., Abramowicz, M. A., Lasota, J.-P., Narayan, R., & Yi, I. 1995, ApJ, 443, L61
- Czerny, B. 2019, Universe, 5, 131
- Done, C., Gierliński, M., & Kubota, A. 2007, A&A Rev., 15, 1
- Du, P., Zhang, Z.-X., Wang, K., et al. 2018, ApJ, 856, 6
- Giustini, M., Rodríguez Hidalgo, P., Reeves, J. N., et al. 2023, A&A, 679, A73
- Grzędzielski, M., Janiuk, A., Czerny, B., & Wu, Q. 2017, A&A, 603, A110
- Habibi, A. & Abbassi, S. 2019, ApJ, 887, 256
- Hawley, J. F., Gammie, C. F., & Balbus, S. A. 1995, ApJ, 440, 742
- Hirose, S., Krolik, J. H., & Blaes, O. 2009, ApJ, 691, 16
- Hutsemékers, D. & Sluse, D. 2025, A&A, 695, A10
- Janiuk, A. & Czerny, B. 2011, MNRAS, 414, 2186
- Jha, V. K., Joshi, R., Chand, H., et al. 2022, MNRAS, 511, 3005
- Jiang, Y.-F., Blaes, O., Stone, J. M., & Davis, S. W. 2019, ApJ, 885, 144
- Jiang, Y.-F., Davis, S. W., & Stone, J. M. 2016, The Astrophysical Journal, 827, 10
- Jiang, Y.-F., Stone, J. M., & Davis, S. W. 2013a, ApJ, 778, 65
- Jiang, Y.-F., Stone, J. M., & Davis, S. W. 2013b, ApJ, 767, 148
- Kelly, B. C., Bechtold, J., & Siemiginowska, A. 2009, ApJ, 698, 895
- King, A. R., Pringle, J. E., & Livio, M. 2007, MNRAS, 376, 1740
- Laor, A. & Davis, S. W. 2014, MNRAS, 438, 3024
- Leung, G. C. K., Eilers, A.-C., Panagiotou, C., et al. 2026, Discovery of Quasar Variability and Early Accretion Disk Signatures at Cosmic Dawn
- Lightman, A. P. & Eardley, D. M. 1974, ApJ, 187, L1
- McHardy, I. M., Koording, E., Knigge, C., Uttley, P., & Fender, R. P. 2006, Nature, 444, 730
- Merloni, A. & Nayakshin, S. 2006, MNRAS, 372, 728
- Morgan, C. W., Kochanek, C. S., Morgan, N. D., & Falco, E. E. 2010, ApJ, 712, 1129
- Mosallanezhad, A., Abbassi, S., & Beiranvand, N. 2014, MNRAS, 437, 3112
- Murray, N., Chiang, J., Grossman, S. A., & Voit, G. M. 1995, ApJ, 451, 498
- Narayan, R. & Yi, I. 1994, The Astrophysical Journal, 428, L13
- Netzer, H. 2013, The Physics and Evolution of Active Galactic Nuclei (Cambridge, UK: Cambridge University Press)
- Penna, R. F., Sądowski, A., Kulkarni, A. K., & Narayan, R. 2013, MNRAS, 428, 2255
- Piran, T. 1978, ApJ, 221, 652
- Poutanen, J., Lipunova, G., Fabrika, S., Butkevich, A. G., & Abolmasov, P. 2007, MNRAS, 377, 1187
- Pringle, J. E. 1981, ARA&A, 19, 137
- Proga, D., Stone, J. M., & Kallman, T. R. 2000, ApJ, 543, 686
- Sądowski, A. 2016a, MNRAS, 462, 960
- Sądowski, A. 2016b, MNRAS, 459, 4397
- Sakimoto, P. J. & Coroniti, F. V. 1981, ApJ, 247, 19
- Shakura, N. I. & Sunyaev, R. A. 1973, A&A, 500, 33
- Shakura, N. I. & Sunyaev, R. A. 1976, MNRAS, 175, 613
- Sniegowska, M., Grzędzielski, M., Czerny, B., & Janiuk, A. 2023, A&A, 672, A19
- Stella, L. & Rosner, R. 1984, ApJ, 277, 312
- Stone, Z., Shen, Y., Burke, C. J., et al. 2022, MNRAS, 514, 164
- Wang, J.-M., Qiu, J., Du, P., & Ho, L. C. 2014, ApJ, 797, 65
- Zheng, S.-M., Yuan, F., Gu, W.-M., & Lu, J.-F. 2011, ApJ, 732, 52

## Appendix A: TD stability condition

In the present framework,  $\alpha$  is no longer constant, but

$$\alpha = \alpha_x, \quad (\text{A.1})$$

and it depends locally on the thermodynamic state via

$$X \equiv P_{\text{gas}} / P_{\text{rad}}. \quad (\text{A.2})$$

Any change in  $X$  is thus reflected in value of  $\alpha$ , i.e.

$$\delta \ln \alpha = \eta_x \delta \ln X, \quad (\text{A.3})$$

or, equivalently,

$$\eta_x = d \ln \alpha / d \ln X. \quad (\text{A.4})$$

### A.1. Basic equations

The following fundamental equations describe a steady, Keplerian, optically thick structure.

(a) Vertical hydrostatic equilibrium:

$$P_{\text{tot}} = \Omega_K^2 \Sigma H / 2, \quad (\text{A.5})$$

10 where  $\Omega_K = (GM/R^3)^{1/2}$  is the Keplerian angular velocity, and  $\Sigma = 2\rho H$  is the surface density, where  $\rho$  is the midplane density, and  $H$  is the pressure scale height.

$$P_{\text{tot}} = P_{\text{gas}} + P_{\text{rad}}, \quad (\text{A.6})$$

is the total midplane pressure consisting of gas pressure and radiation pressure, where

$$P_{\text{gas}} = (k_B/m_H) \Sigma T_c H^{-1}, \quad (\text{A.7})$$

$$P_{\text{rad}} = a T_c^4 / 3, \quad (\text{A.8})$$

where  $a$  is the radiation constant,  $k_B$  the Boltzmann constant, and  $m_H$  is the hydrogen mass.

(b) Angular momentum transport

$$3\pi \nu \Sigma = \dot{M} \mathcal{J}(R), \quad (\text{A.9})$$

20 where  $\dot{M}$  is the accretion rate,  $\nu = \alpha c_s H$  is the kinematic viscosity,  $c_s = \Omega_K H$  is the sound speed, and  $\mathcal{J} = 1 - \sqrt{R_{\text{in}}/R}$  is the inner boundary correction.

(c) Energy balance

$$Q_{\text{vis}} = Q_{\text{rad}} + Q_{\text{adv}}, \quad (\text{A.10})$$

i.e. viscous dissipation balances cooling through radiation and advection, where

$$Q_{\text{vis}} = 3 \Omega_K H \alpha P_{\text{tot}} / 2, \quad (\text{A.11})$$

$$Q_{\text{rad}} = \frac{32\sigma T_c^4}{3\tau}, \quad (\text{A.12})$$

$$Q_{\text{adv}} = \frac{\mu \dot{M} \Omega_K^2 H^2}{2\pi R^2}, \quad (\text{A.13})$$

where  $T_c$  is the midplane temperature, and  $\tau = \kappa \Sigma / 2$  is the vertical optical depth, with  $\kappa$  for the opacity.

### A.2. Thermal stability analysis with $\alpha_x$

For an infinitesimal temperature perturbation while  $\Sigma$  is taken to be constant, thermal stability requires 30

$$(\partial [Q_{\text{vis}} - Q_{\text{rad}} - Q_{\text{adv}}] / \partial T)_{\Sigma} < 0, \quad (\text{A.14})$$

or, since  $T > 0$ , simply

$$\delta Q_{\text{vis}} - \delta Q_{\text{rad}} - \delta Q_{\text{adv}} < 0. \quad (\text{A.15})$$

Defining

$$f_a \equiv Q_{\text{adv}} / Q_{\text{vis}}, \quad f_r \equiv Q_{\text{rad}} / Q_{\text{vis}}, \quad f_r + f_a = 1, \quad (\text{A.16})$$

Then

$$Q_{\text{vis}} [\delta \ln Q_{\text{vis}} - f_r \delta \ln Q_{\text{rad}} - f_a \delta \ln Q_{\text{adv}}] < 0 \quad (\text{A.17})$$

Since  $Q_{\text{vis}} > 0$ , the sign is set only by the bracket.

The dissipative heating, diffusive radiative cooling, the advective cooling terms

$$\delta \ln Q_{\text{vis}} = \delta \ln \alpha + \delta \ln P_{\text{tot}} + \delta \ln H,$$

$$\delta \ln Q_{\text{rad}} = 4 \delta \ln T,$$

$$\delta \ln Q_{\text{adv}} = \delta \ln \dot{M} + 2 \delta \ln H. \quad (\text{A.18})$$

In order to proceed, we define

$$\beta_r \equiv P_{\text{rad}} / P_{\text{tot}}, \quad \beta_g \equiv P_{\text{gas}} / P_{\text{tot}}, \quad \beta_r + \beta_g = 1. \quad (\text{A.19})$$

Therefore, at a given radius for a fixed  $\Sigma$ ,

$$\delta \ln P_{\text{tot}} = \delta \ln H,$$

$$\delta \ln P_{\text{tot}} = \beta_r \delta \ln P_{\text{rad}} + \beta_g \delta \ln P_{\text{gas}},$$

$$\delta \ln P_{\text{gas}} = \delta \ln T - \delta \ln H,$$

$$\delta \ln P_{\text{rad}} = 4 \delta \ln T, \quad (\text{A.20})$$

so

$$\delta \ln H = A \delta \ln T / D, \quad (\text{A.21})$$

where

$$A \equiv 4 - 3\beta_g, \quad D \equiv 1 + \beta_g, \quad (\text{A.22})$$

Using  $X \equiv P_{\text{gas}} / P_{\text{rad}}$ , we have

$$\delta \ln X = \delta \ln P_{\text{gas}} - \delta \ln P_{\text{rad}}, \quad (\text{A.23})$$

which, combined with Eqs. A.3, A.20, and A.21, yields

$$\delta \ln \alpha = -7\eta_x \delta \ln T / D \quad (\text{A.24})$$

Using the angular-momentum equation

$$\delta \ln \dot{M} = \delta \ln \alpha + \delta \ln P_{\text{tot}} + \delta \ln H,$$

$$20 \quad \delta \ln \dot{M} = (2A - 7\eta_x) \delta \ln T / D \quad (\text{A.25})$$

Now substituting into Eq. (A.18):

$$\delta \ln Q_{\text{vis}} = (2A - 7\eta_x) \delta \ln T / D,$$

$$\delta \ln Q_{\text{adv}} = (4A - 7\eta_x) \delta \ln T / D. \quad (\text{A.26})$$

Then

$$\left[ \frac{2A - 7\eta_x}{D} - 4f_r - f_a \frac{4A - 7\eta_x}{D} \right] \delta \ln T < 0. \quad (\text{A.27})$$

For a positive temperature perturbation,  $\delta \ln T > 0$ , and as  $D$  is always positive, stability condition reads as

$$\Delta = 2A - 4D + 4f_a(D - A) - 7(1 - f_a)\eta_x < 0, \quad (\text{A.28})$$

The most unstable regime corresponds to

$$\beta_g \rightarrow 0, \quad f_a \rightarrow 0, \quad (\text{A.29})$$

thus, stability requires

$$\Delta = 4 - 7\eta_x < 0, \quad (\text{A.30})$$

$$\eta_x > 4/7 \approx 0.571. \quad (\text{A.31})$$

### A.3. Constraining $\alpha_x$ from the $\dot{M}$ - $\Sigma$ relation

We now specialize to the RPD, radiatively cooled regime,

$$P_{\text{rad}} \gg P_{\text{gas}}, \quad Q_{\text{adv}} \ll Q_{\text{rad}}, \quad (\text{A.32})$$

in which the classical thermal–viscous instability arises. We derive a general constraint on the functional form of the viscosity  $\alpha_x$  from the structure of the  $\dot{M}$ - $\Sigma$  equilibrium curve, without assuming a specific parametric form. At fixed radius, the unstable branch lies in this regime, allowing the following scalings.

From vertical hydrostatic equilibrium,

$$P_{\text{tot}} \propto \Sigma H, \quad (\text{A.33})$$

and in the RPD limit,

$$P_{\text{tot}} \approx P_{\text{rad}} \propto T^4, \quad (\text{A.34})$$

which gives

$$H \propto T^4 \Sigma^{-1}. \quad (\text{A.35})$$

The gas pressure scales as

$$P_{\text{gas}} \propto \rho T \propto \Sigma T H^{-1}, \quad (\text{A.36})$$

and therefore

$$P_{\text{gas}} \propto \Sigma^2 T^{-3}. \quad (\text{A.37})$$

Combining these expressions, we obtain

$$X \equiv P_{\text{gas}}/P_{\text{rad}} \propto \Sigma^2 T^{-7}. \quad (\text{A.38})$$

The viscous heating rate scales as

$$Q_{\text{vis}} \propto \alpha P_{\text{tot}} H \propto \alpha T^8 \Sigma^{-1}, \quad (\text{A.39})$$

while radiative cooling gives

$$Q_{\text{rad}} \propto T^4 \Sigma^{-1}. \quad (\text{A.40})$$

Thermal equilibrium  $Q_{\text{vis}} = Q_{\text{rad}}$  then implies  $\alpha T^4 = \text{const.}$ , hence,  $T^4 \propto \alpha^{-1}$ . Substituting into the expression for  $X$  yields

$$X \propto \Sigma^2 \alpha^{7/4}, \quad (\text{A.41})$$

which determines  $X(\Sigma)$  along the equilibrium branch

Taking the logarithm of the constraint equation,

$$\ln X - \frac{7}{4} \ln \alpha_x = 2 \ln \Sigma + \text{const}, \quad (\text{A.42})$$

and differentiating with respect to  $\ln \Sigma$ , we obtain

$$d \ln X / d \ln \Sigma = 8 / (4 - 7\eta_x). \quad (\text{A.43})$$

From angular momentum transport,

$$\dot{M} \propto \alpha P_{\text{tot}} H \propto \alpha T^8 \Sigma^{-1}. \quad (\text{A.44})$$

Using the thermal equilibrium condition, we obtain

$$\dot{M} \propto \alpha_x^{-1} \Sigma^{-1}. \quad (\text{A.45})$$

Thus, the full  $\dot{M}(\Sigma)$  relation is determined by the implicit dependence  $X(\Sigma)$ .

Differentiating  $\ln \dot{M}$  gives

$$d \ln \dot{M} / d \ln \Sigma = -1 - \eta_x d \ln X / d \ln \Sigma. \quad (\text{A.46})$$

Substituting, we find

$$d \ln \dot{M} / d \ln \Sigma = (\eta_x + 4) / (7\eta_x - 4). \quad (\text{A.47})$$

This equation gives the general slope of the  $\dot{M}$ - $\Sigma$  equilibrium curve for an arbitrary  $\alpha_x$ . The classical instability corresponds to the denominator changing sign, producing a negative-slope segment. Requiring  $d \ln \dot{M} / d \ln \Sigma > 0$ , yields a necessary condition for the absence of the unstable branch. For  $\eta_x > 0$ , this implies

$$\eta_x > 4/7 \approx 0.571. \quad (\text{A.48})$$

### A.4. Implications for $\alpha_x$

A simple sufficient prescription satisfying the stability condition derived above is a power-law form

$$\alpha_x = \alpha_0 X^p, \quad p > 4/7 \quad (\text{A.49})$$

where  $\alpha_0$  is a normalization constant setting the overall amplitude of the effective viscosity.

Hence, the requirement of a single-valued thermally stable equilibrium solution directly implies that viscosity must increase sufficiently steeply with  $X$ . The functional form of  $\alpha_x$  is thus not arbitrary, but imposed by internal consistency of TD equations.

The power-law form should be interpreted as the local response of the effective viscosity to the pressure partition, rather than a global prescription for its absolute value. In practice,  $\alpha$  remains bounded, since  $X$  is finite across disk regimes, and the normalization  $\alpha_0$  can be chosen to keep  $\alpha$  within the empirically expected range. We adopt  $X \equiv P_{\text{gas}}/P_{\text{rad}}$ , so that RPD regions correspond to  $X \ll 1$ . This choice is arbitrary up to inversion: defining instead  $P_{\text{rad}}/P_{\text{gas}}$  would lead to an equivalent constraint with reversed sign, without affecting the physical conclusion.

### A.5. Structural changes with $\alpha_x$

The total pressure can be written as

$$P_{\text{tot}} = P_{\text{rad}} + P_{\text{gas}} = P_{\text{rad}}(1 + X) \propto T^4(1 + X). \quad (\text{A.50})$$

From vertical hydrostatic balance,

$$T^4 \propto \Omega_K^2 \Sigma H (1 + X)^{-1}, \quad (\text{A.51})$$

and from angular momentum transport,

$$\Sigma \propto \dot{M} \mathcal{J} \alpha^{-1} \Omega_K^{-1} H^{-2}. \quad (\text{A.52})$$

Now using  $X \propto \Sigma H^{-1} T^{-3}$ , one obtains

$$H^9 \propto \dot{M} \mathcal{J} \Omega_K^{-7} \alpha^{-1} X^{-4} (1 + X)^3, \quad (\text{A.53})$$

$$T_c^9 \propto \dot{M}^2 \mathcal{J}^2 \Omega_K^4 \alpha^{-2} X (1 + X)^{-3}, \quad (\text{A.54})$$

$$\Sigma^9 \propto \dot{M}^7 \mathcal{J}^7 \Omega_K^5 \alpha^{-7} X^8 (1 + X)^{-6}. \quad (\text{A.55})$$

Moreover, the energy balance ( $Q_{\text{vis}} = Q_{\text{rad}} + Q_{\text{adv}}$ ) leads to a quadratic equation for  $H$ ,

$$H^2 + \frac{8\pi c R^2}{\kappa \dot{M} (1 + X)} H - \frac{\mathcal{J} R^2}{2\mu} = 0, \quad (\text{A.56})$$

yielding, to leading order,

$$H \propto \kappa \dot{M} \mathcal{J} (1 + X), \quad (\text{A.57})$$

thus,

$$X^4 (1 + X)^6 \propto \kappa^{-9} \dot{M}^{-8} \mathcal{J}^{-8} \alpha^{-1} \Omega_K^{-7}. \quad (\text{A.58})$$

At given  $R$ ,  $M$ , and  $\dot{M}$ , the logarithmic differences between the solutions are

$$\delta \ln H = \delta \ln \kappa + \delta \ln (1 + X), \quad (\text{A.59})$$

$$9 \delta \ln H = -4 \delta \ln X + 3 \delta \ln (1 + X) - \delta \ln \alpha, \quad (\text{A.60})$$

$$9 \delta \ln T = \delta \ln X - 3 \delta \ln (1 + X) - 2 \delta \ln \alpha, \quad (\text{A.61})$$

$$9 \delta \ln \Sigma = 8 \delta \ln X - 6 \delta \ln (1 + X) - 7 \delta \ln \alpha, \quad (\text{A.62})$$

$$4 \delta \ln X + 6 \delta \ln (1 + X) = -9 \delta \ln \kappa - \delta \ln \alpha. \quad (\text{A.63})$$

We compare the TD structures obtained with  $\alpha_x$  to those of the SS model using the differential logarithmic relations we just found (Eqs. A.59–A.63), focusing on the inner regions dominated by electron-scattering opacity,  $\kappa = \kappa_{\text{es}}$ ,

$$6 \delta \log H = \mathcal{A} - 4 \delta \log X, \quad (\text{A.64})$$

$$6 \delta \log T = \mathcal{A} + 2 \delta \log X, \quad (\text{A.65})$$

$$3 \delta \log \Sigma = 2 \mathcal{A} + 4 \delta \log X, \quad (\text{A.66})$$

$$4 \delta \log X + 6 \delta \log(1 + X) = \mathcal{A}, \quad (\text{A.67})$$

where

$$\mathcal{A} = -\delta \log \alpha = \log \alpha_{\text{ss}} - \log \alpha_0 - p \log X_x. \quad (\text{A.68})$$

This yields

$$(4 + p) \delta \log X + 6 \delta \log(1 + X) = \log(\alpha_{\text{ss}}/\alpha_0) - p \log X_{\text{ss}}. \quad (\text{A.69})$$

From Eq. A.58, we have

$$X^4 (1 + X)^6 = C S^{-1} \alpha^{-1}, \quad (\text{A.70})$$

where  $C_0 \simeq 10^{-23} (\eta/0.1)^8 (\kappa/0.34)^{-9} (\mu_m/0.615)^{-4}$ , collects physical constants, and dimensionless parameter  $S$  is given by

$$S = \dot{m}^8 M_\bullet \mathcal{J}^8(r) r^{-21/2}. \quad (\text{A.71})$$

This gives,

$$\log X_{\text{ss}} = (\log C - \log S - \log \alpha_{\text{ss}}) / q, \quad (\text{A.72})$$

where  $q = 4$  and  $q = 10$ , in RPD ( $X \ll 1$ ) and GPD ( $X \gg 1$ ) regions, respectively.

From Eq. A.59, we further note that in the RPD regime  $\delta \log H \simeq 0$ , but in the GPD regime  $\delta \log H \simeq \delta \log X$ . This shows that the  $\alpha_x$  prescription largely preserves the geometrically thin structure of the disk.

The structural scalings then reduce to

$$\delta \log \Sigma = 4 \delta \log T = 4 \delta \log X = \mathcal{A}_{\text{rad}}, \quad (\text{A.73})$$

$$\delta \log \Sigma = 4 \delta \log T = 8 \delta \log H = 8 \delta \log X = 0.8 \mathcal{A}_{\text{gas}}, \quad (\text{A.74})$$

where the regime-dependent  $\mathcal{A}$  is

$$\mathcal{A} = \frac{p \log S + (p + q) \log \alpha_{\text{ss}} - q \log \alpha_0 + 23 p}{(p + q)}. \quad (\text{A.75})$$

For  $\alpha_{\text{ss}} = 0.1$ , this becomes

$$\mathcal{A} = \frac{p}{(p + q)} (\log S + 22) - \frac{q}{(p + q)} (\log \alpha_0 + 1). \quad (\text{A.76})$$

The resulting  $\mathcal{A}$ , the logarithmic deviation from SS model, provides an accurate description for  $\log \dot{m} \gtrsim -1$ , where the optically thick radiative cooling assumption holds, and for  $\log M_\bullet \gtrsim 4$ , where the quadratic solution for  $H$  remains valid.

Figure A.1 shows how the deviation parameter  $\mathcal{A}$  (Sec. A.5), which measures the logarithmic differences between the  $\alpha_x$  and  $\alpha_{\text{ss}}$  solutions, varies with radius for representative  $p$ . It follows the analytic scaling in Eq. A.76, depending on both  $S$  and  $p$ , with  $q$  weighting the two pressure regimes. In the RPD regime, the solid curves show  $\mathcal{A} > 0$  over a broad radial range, implying higher temperatures and surface densities than in the SS model. The deviation grows in magnitude and radial extent with  $p$ , reflecting the stronger sensitivity of viscosity to pressure partition. In the GPD regime, the dashed curves decline with radius, eventually crossing zero and becoming negative, indicating lower

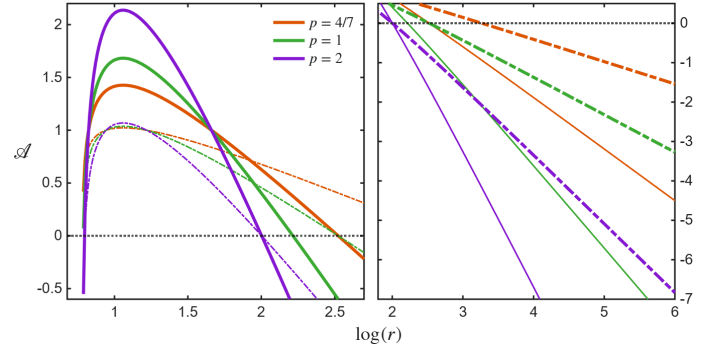


**Fig. A.1.** Radial behavior of the logarithmic deviation parameter  $\mathcal{A}$  for  $M_\bullet = 10^6$  and  $\dot{m} = 0.1$ , with  $\kappa = \kappa_{\text{es}}$ . Solid curves correspond to the RPD scaling ( $\mathcal{A}_{\text{rad}}$  with  $q = 4$ ), while dashed curves represent the GPD regime ( $\mathcal{A}_{\text{gas}}$  with  $q = 10$ ). The right panel extends the left panel. Different colors indicate the slope  $p$  of the viscosity law, with  $\alpha_0 = 0.01$ . The horizontal dotted line marks  $\mathcal{A} = 0$ , corresponding to no deviation from the standard SS solution.

structural quantities than in the SS solutions. Since  $X$  increases outward (Eq. A.70), the RPD and GPD regimes correspond to the inner and outer disk, respectively. The figure also shows that the radial profiles steepen with increasing  $p$ . For the marginally stable case,  $p = 4/7$ , the deviations are mild and extend over a broad radial range, whereas larger  $p$  produces stronger and more localized deviations, yielding a sharper RPD-GPD transition as  $\mathcal{A}$  declines rapidly toward the outer disk.

Since  $\alpha_x$  reduces the sensitivity of heating to the RPD state and increases  $\Sigma$  and  $\tau$ , it should produce a more slowly evolving inner flow. In the present model,

$$\delta \log t_{\text{thermal}} = \delta \log t_{\text{inflow}} = -\delta \log \alpha = \mathcal{A}_{\text{rad}}, \quad (\text{A.77})$$

which is positive over a broad range of inner disk radii, as shown in Fig. A.1.

Overall, the  $\alpha_x$  prescription preserves the geometrically thin disk structure while introducing controlled, regime-dependent changes in the thermodynamic variables. These changes remain continuous across the RPD-GPD transition, reflecting the removal of the multi-valued unstable branch.

#### A.6. Asymptotic structural scaling solutions with $\alpha_x$

We now examine how the  $\alpha_x$  prescription modifies the asymptotic TD scalings. The effective viscosity varies with the local pressure partition. This changes the response of disk structure to the system global parameters (Eq. A.58), as

$$X \propto (\alpha_0 \kappa^9 \dot{M}^8 \mathcal{J}^8 \Omega_K^7)^{-1/(q+p)}, \quad (\text{A.78})$$

where  $q = 4$  and  $q = 10$ , in RPD ( $X \ll 1$ ) and GPD ( $X \gg 1$ ) regions, respectively.

Thus, compared with the  $\alpha_{\text{ss}}$  case, the dependence of  $X$  power on the system global parameters is weakened from  $q^{-1}$  to  $(q + p)^{-1}$ .

The disk thickness in RPD regime, follows from substituting the asymptotic solution for  $X$ , yielding

$$H_{\text{rad}} \propto \kappa \dot{M} \mathcal{J}. \quad (\text{A.79})$$

Therefore, in this limit, the explicit dependence on  $\alpha_0$  and  $p$  cancels from the leading-order thickness scaling. The main

180 structural changes instead appear in the mid-plane temperature, and surface density, as

$$T_{\text{rad}} \propto (\kappa^{2p-1} \dot{M}^{2p} \mathcal{J}^{2p} \Omega_K^{2p+1} \alpha_0^{-1})^{1/(4+p)}, \quad (\text{A.80})$$

$$\Sigma_{\text{rad}} \propto (\kappa^{7p-8} \dot{M}^{7p-4} \mathcal{J}^{7p-4} \Omega_K^{6p-4} \alpha_0^{-4})^{1/(4+p)}. \quad (\text{A.81})$$

Thus, in the RPD branch, the  $\alpha_x$  prescription mainly redistributes the classical dependence of  $T_c$  and  $\Sigma$  on the disk system global parameters and on the viscosity normalization  $\alpha_0$ . Since  $X \ll 1$ , a positive  $p$  implies  $\alpha_x = \alpha_0 X^p < \alpha_0$ , leading to a reduced effective viscosity in the RPD part of the disk.

In the opposite, GPD limit, we end up with

$$H_{\text{rad}} \propto (\kappa^{p+1} \dot{M}^{p+2} \mathcal{J}^{p+2} \Omega_K^{-7} \alpha_0^{-1})^{1/(10+p)}, \quad (\text{A.82})$$

$$T_{\text{rad}} \propto (\kappa^{2p+2} \dot{M}^{2p+4} \mathcal{J}^{2p+4} \Omega_K^{2p+6} \alpha_0^{-2})^{1/(10+p)}, \quad (\text{A.83})$$

$$\Sigma_{\text{rad}} \propto (\kappa^{7p-2} \dot{M}^{7p+6} \mathcal{J}^{7p+6} \Omega_K^{6p+4} \alpha_0^{-8})^{1/(10+p)}. \quad (\text{A.84})$$

190 These asymptotic relations show explicitly where the new closure departs from the classical  $\alpha_{\text{ss}}$  solution. The modification does not simply rescale the SS disk by a constant factor; rather, it changes the local power-law response of the disk structure through the pressure ratio.

The dimensionless form of asymptotic scaling relations derived under the  $\alpha_x$  prescription, separated into three main regimes analogous to the standard SS-disk regions, are presented in the following

#### A.6.1. Region A: RPD ( $X \ll 1$ ), with $\kappa_{\text{es}}$

$$H \propto \dot{m} \mathcal{J} M. \quad (\text{A.85})$$

$$H/R \propto \dot{m} \mathcal{J} r^{-1} \quad (\text{A.86})$$

$$T_c \propto (M_{\bullet}^{-1} (\dot{m} \mathcal{J})^{2p} r^{-3p-3/2} \alpha_0^{-1})^w \quad (\text{A.87})$$

$$\Sigma \propto (M_{\bullet}^p (\dot{m} \mathcal{J})^{7p-4} r^{-9p+6} \alpha_0^{-4})^w \quad (\text{A.88})$$

$$\rho \propto (M_{\bullet}^{-4} (\dot{m} \mathcal{J})^{6p-8} r^{-9p+6} \alpha_0^{-4})^w \quad (\text{A.89})$$

$$P \propto (M_{\bullet}^{-1} (\dot{m} \mathcal{J})^{2p} r^{-3p-3/2} \alpha_0^{-1})^{4w} \quad (\text{A.90})$$

$$X \propto (M_{\bullet}^{-1} (\dot{m} \mathcal{J})^{-8} r^{21/2} \alpha_0^{-1})^w \quad (\text{A.91})$$

with  $w = 1/(4 + p)$ .

#### A.6.2. Region B: GPD ( $X \gg 1$ ), with $\kappa_{\text{es}}$

$$H \propto (M_{\bullet}^{p+9} (\dot{m} \mathcal{J})^{p+2} r^{21/2} \alpha_0^{-1})^w \quad (\text{A.92})$$

$$H/R \propto (M_{\bullet}^{-1} (\dot{m} \mathcal{J})^{p+2} r^{1/2-p} \alpha_0^{-1})^w \quad (\text{A.93})$$

$$T_c \propto (M_{\bullet}^{-2} (\dot{m} \mathcal{J})^{2p+4} r^{-3p-9} \alpha_0^{-2})^w \quad (\text{A.94})$$

$$\Sigma \propto (M_{\bullet}^{p+2} (\dot{m} \mathcal{J})^{7p+6} r^{-9p-6} \alpha_0^{-8})^w \quad (\text{A.95})$$

$$\rho \propto (M_{\bullet}^{-7} (\dot{m} \mathcal{J})^{6p+4} r^{33/2-9p} \alpha_0^{-7})^w \quad (\text{A.96})$$

$$P \propto (M_{\bullet}^{-9} (\dot{m} \mathcal{J})^{8p+8} r^{15/2-12p} \alpha_0^{-9})^w \quad (\text{A.97})$$

$$X \propto (M_{\bullet}^{-1} (\dot{m} \mathcal{J})^{-8} r^{21/2} \alpha_0^{-1})^w \quad (\text{A.98})$$

with  $w = 1/(10 + p)$ .

#### A.6.3. Region C: GPD ( $X \gg 1$ ), with $\kappa_{\text{ff}}$

200

In this region, the opacity is dominated by bound-free/free-free absorption (Kramers opacity) which has the form  $\kappa_{\text{ff}} \propto \rho T^{-7/2}$ .

$$H \propto (M_{\bullet}^{p+9} (\dot{m} \mathcal{J})^{(p+3)/2} r^{3(p+15)/4} \alpha_0^{-1})^w \quad (\text{A.99})$$

$$H/R \propto (M_{\bullet}^{-1} (\dot{m} \mathcal{J})^{p+2} r^{-(p-5)/4} \alpha_0^{-1})^w \quad (\text{A.100})$$

$$T_c \propto (M_{\bullet}^{-2} (\dot{m} \mathcal{J})^{p+3} r^{-3(p+5)/2} \alpha_0^{-2})^w \quad (\text{A.101})$$

$$\Sigma \propto (M_{\bullet}^{p+2} (\dot{m} \mathcal{J})^{7(p+2)/2} r^{-15(p+2)/4} \alpha_0^{-8})^w \quad (\text{A.102})$$

$$\rho \propto (M_{\bullet}^{-7} (\dot{m} \mathcal{J})^{3p+11/2} r^{-(18p-75)/4} \alpha_0^{-7})^w \quad (\text{A.103})$$

$$P \propto (M_{\bullet}^{-9} (\dot{m} \mathcal{J})^{4p+17/2} r^{-6p-105/4} \alpha_0^{-9})^w \quad (\text{A.104})$$

$$X \propto (M_{\bullet}^{-1} (\dot{m} \mathcal{J})^{-7/2} r^{15/4} \alpha_0^{-1})^w \quad (\text{A.105})$$

with  $w = 1/(10 + p)$ .

The classic SS asymptotic behavior is recovered for  $p = 0$ , and the TD becomes globally stable for  $p > 4/7$ .

210 It also reduces to the prescription of Sakimoto & Coroniti (1981) for  $p = 1$ , because in the RPD regime,  $P_{\text{rad}} \gg P_{\text{gas}}$ , so  $P_{\text{tot}} \simeq P_{\text{rad}}$ , and therefore  $T_{r\phi} \propto \alpha_0 P_{\text{gas}}$ . The key point, however, is that unlike Sakimoto & Coroniti (1981), who directly imposed gas-pressure scaling, the present closure,  $\alpha_x = \alpha_0 X^p$ , emerges from the TD consistency requirement and recovers a gas-pressure-like stress only as the  $p = 1$  RPD-limit case.